Calculation of solid-fluid phase equilibria for systems of chain molecules

James M. Polson and Daan Frenkel
FOM Institute for Atomic and Molecular Physics, Kruislaan 407, 1098 SJ Amsterdam, The Netherlands

(Received 9 February 1998; accepted 26 March 1998)

We study the first order solid-fluid phase transition of a system of semi-flexible Lennard-Jones chains using molecular dynamics simulations. Thermodynamic integration methods are used to calculate the free energy of the solid and fluid phases. The solid phase free energy per chain can be calculated to an accuracy of $\pm 0.03 k_B T$ with relative ease. The Gibbs-Duhem integration technique is used to trace out the complete melting curve, starting with a single point on the curve obtained from the free energy calculations. For the short chains studied here, we find that increasing the chain length stabilizes the solid phase; i.e., it raises the melting temperature at fixed pressure, and lowers the density at the transition at fixed temperature. Gibbs-Duhem integration was used also to investigate the effects of chain stiffness on the transition. We find that increasing the stiffness also acts to stabilize the solid phase. At fixed temperature, the transition is shifted to lower pressure and lower density with increasing chain stiffness. Further, we find that the density gap between solid and fluid broadens with increasing chain stiffness. © *1998 American Institute of Physics*.
[S0021-9606(98)50825-2]

I. INTRODUCTION

Phase transitions between solid and fluid phases are typically strongly first order and characterized by a high degree of hysteresis in the equation of state. For this reason, the determination of the equilibrium coexistence by computer simulation requires special techniques which are suitable for high densities. While a method such as the Gibbs ensemble technique[1] provides a direct means to simulate coexisting phases, this method relies on the exchange of particles between the phases in separate simulation cells, a move which is efficient only at sufficiently low densities. Instead, the calculation of the chemical potential as a function of density in the mechanically stable regions of each phase is required. The coexistence can then be calculated from the basic criterion that temperatures, pressures and chemical potentials of coexisting phases are equal. One approach to calculating the chemical potential is the Widom test particle insertion technique.[2,3] Once again, however, this is a technique which relies on insertion of particles into the system; in this case, one calculates the average of the Boltzmann factor corresponding to the change in potential energy upon insertion of a test particle. At high densities, only very few test insertions will have a non-negligible Boltzmann weight, leading to a large statistical error in the calculation of the average. There is an additional complication in the case of a crystalline solid: random insertion of a test particle into an N-particle crystal results in the formation of an interstitial rather than a crystal with $N+1$ lattice sites.

An alternative approach to the calculation of the chemical potential is the calculation of the Helmholtz free energy via thermodynamic integration. The essential idea behind thermodynamic integration is the transformation of the system from one state to another of known free energy, and to calculate the free energy difference involved in the transformation. For example, the free energy of a fluid at arbitrary density can be calculated by integration along an isotherm to zero density, at which the system behaves as an ideal gas of known free energy. Obviously, such a method cannot be applied to the solid phase since expansion of the system carries it through the first-order melting transition, a nonreversible path through which the free energy cannot be integrated. An alternative route is to cool the solid at constant density to a low-temperature harmonic solid. The free energy of this state can be calculated analytically, and the free energy difference between the two states is related to the integral of the internal energy along the isochore. However, this approach can be hampered by the presence of solid-solid phase transitions along the isochore. Further, it is not suitable for particles interacting with discontinuous potentials which do not form harmonic solids at low temperatures. Finally, there is an additional problem in the case of complex molecules: even if the system can be cooled to become a harmonic crystal, the calculation of the Helmholtz free energy in this limit is highly nontrivial.

Rather than performing thermodynamic integrations along *natural* pathways such as isotherms and isochores, it is possible and more convenient to perform an analogous integration along *artificial* reversible pathways. This involves the variation, not of state variables such as temperature and density, but of the actual particle interactions, to transform the system to a state of known free energy. An early application of artificial thermodynamic integration to calculate the free energy of simple atomic solids was the single-occupancy-cell method introduced by Hoover and Ree in 1968, which was also applied to the hard-sphere solid.[4] Later, however, some technical problems with this method were discovered.[5] An alternative and more general method to calculate the free energy of arbitrary atomic solids was introduced by Frenkel and Ladd in 1984.[6] The method involves the transformation of the atomic solid to a lattice-coupled solid by gradually imposing an interaction coupling

the atoms to their lattice sites, and, in the case of particles with continuous potentials, the simultaneous removal of interparticle interactions. A convenient reference solid is the Einstein crystal, in which particles are harmonically coupled to their lattice sites. The free energy of the Einstein crystal is known, and the free energy difference associated with the transformation can be calculated in a straightforward manner. The method was originally applied to the hard sphere solid to calculate the free energy difference between face-centered-cubic (fcc) and hexagonal-close-packed (hcp) lattices,[6] a calculation that has been repeated recently to a higher degree of accuracy.[7,8] Later, this method was extended for use for particles with orientational degrees of freedom as well. In this case, the coupling of the particle positions to the lattice sites is augmented by an external field which induces orientational alignment. This approach has been applied to calculate solid phase free energies required for the calculation of the phase diagrams of hard ellipsoids[9,10] and hard spherocylinders.[11,12] As well, this method has been applied, with further refinements where necessary, to study the phase behavior of simple molecular solids such as N_2,[13–15] CO_2,[16] N_2O,[17] and H_2O.[18]

An important type of system for which the lattice-coupling free energy calculation method has not yet been applied is that of solids composed of semiflexible chain molecules. In principle, this should involve a relatively straightforward extension of the existing technique. The calculation of the solid phase free energy provides the first step in the determination of the solid-fluid equilibrium phase behavior of chain molecules. Once an initial point on the phase boundary has been determined, the powerful Gibbs-Duhem integration technique[19,20] can be employed to calculate the complete coexistence curve in a way much less computationally demanding than by performing an additional free energy calculation for every new point on the curve. Further, this latter method permits a relatively straightforward means to study the effect of molecular properties such as flexibility on the phase behavior. In the present study, we investigate the application of the lattice-coupling method to an idealized model system composed of chains of Lennard-Jones particles. Clearly, the model is too crude to achieve quantitative agreement with experimental results for real molecular systems. Nevertheless, this approach should provide an effective means to study the generic effects of chain length and chain stiffness on the solid-fluid phase behavior of semiflexible chains. The long term goal of this work, however, is the further refinement of the methods for application to more realistically modeled chain molecule systems.

In Sec. II we describe the theoretical background and methods employed in the present study. In particular, in Sec. II A we describe the details of the molecular model; in Sec. II B, we present theoretical background for the calculation of the free energy in the solid and fluid phases; in Sec. II C, we discuss the application of Gibbs-Duhem integration to calculate the phase boundaries; and in Sec. II D we describe the details of the simulations. In Sec. III, we present and discuss the results. Section IV summarizes the main results of the paper.

II. THEORY AND METHODS

A. Model

The oligomeric chains considered here are semiflexible ''pearl-necklace'' strings of bonded beads. Nonbonded sites interact with a truncated and shifted Lennard-Jones (LJ) interaction,

$$U_{\mathrm{LJ}}(r)=4\epsilon\left[\left(\frac{\sigma}{r}\right)^{12}-\left(\frac{\sigma}{r}\right)^{6}-\left(\frac{\sigma}{r_c}\right)^{12}+\left(\frac{\sigma}{r_c}\right)^{6}\right],$$

$$r<r_c=0, r>r_c\,, \tag{1}$$

where σ and ϵ are the standard LJ parameters, where r is the distance between beads, and r_c is the cutoff distance, which we set at $r_c=2.5\sigma$. Bonded sites are connected with harmonic springs with the following potential:

$$U_{\mathrm{stretch}}(r_i)=\tfrac{1}{2}k_b(r_i-r_b)^2, \tag{2}$$

where r_i is the distance between the $(i-1)^{\mathrm{th}}$ and the i^{th} beads, r_b is the equilibrium bond length, and k_b is the bond-stretching harmonic force constant. We fix $r_b=\sigma$, and, unless otherwise stated, $k_b\sigma^2/\epsilon=500$. Finally, we include a bending potential given by

$$U_{\mathrm{bend}}(\theta_i)=\tfrac{1}{2}k_\theta(\theta_i)^2, \tag{3}$$

where $\theta_i=\cos^{-1}(\hat{u}_{i-1}\cdot\hat{u}_i)$, where $\hat{u}_i$ is the unit vector describing the orientation of the i^{th} bond in the chain, and where k_θ is a bending force constant.

B. Free energy calculations

The solid-fluid transition is strongly first order with a considerable degree of hysteresis in the equation of state. Consequently, it is essential to perform free energy calculations in order to determine the melting curve of the system. The conditions for the equilibrium coexistence are that the temperatures, pressures and chemical potentials of the coexisting phases be equal. The chemical potential is given by,

$$\mu=\frac{F(\rho)}{N_{\mathrm{ch}}}+\frac{nP(\rho)}{\rho}, \tag{4}$$

where F is the Helmholtz free energy of the system, N_{ch} is the total number of chains, $P(\rho)$ is the pressure as a function of the density of monomers $\rho=N/V$, and $n=N/N_{\mathrm{ch}}$ is the number of monomers per chain. If the Helmholtz free energy at a density ρ_0 is known, it can be calculated at any other density ρ by the following relation:

$$\frac{F(\rho)}{N_{\mathrm{ch}}}=\frac{F(\rho_0)}{N_{\mathrm{ch}}}+n\int_{\rho_0}^{\rho}d\rho'\,\frac{P(\rho')}{\rho'^2}. \tag{5}$$

Thus, in order to compute the chemical potentials, one must first calculate the absolute Helmholtz free energy at some reference point ρ_0. The details of this calculation differ for the solid and fluid phases.

1. Solid phase

In order to calculate the Helmholtz free energy of a crystalline solid phase, we employ a variant of the method developed by Frenkel and Ladd,[6] which involves a thermodynamic integration scheme to link a state of a given system along a reversible path to that of another system for which the partition function, and, hence, the Helmholtz free energy, can be calculated analytically. A convenient reference system is the Einstein crystal, where individual noninteracting particles are coupled harmonically to their equilibrium lattice positions,

$$U_{\mathrm{Ein}}=\frac{\alpha}{2}\sum_{i=1}^{N}(\mathbf{R}_i-\mathbf{R}_i^{(0)})^2, \tag{6}$$

where $\mathbf{R}_i$ is the instantaneous position of the i^{th} particle, and $\mathbf{R}_i^{(0)}$ is the corresponding Einstein crystal lattice position. Note that the Einstein crystal lattice is given the same structure as that of the true system. Further, note that a ''particle'' in the context of a system of chains refers to an individual bead on a chain. The partition function and, thus, the Helmholtz free energy of the Einstein crystal of fixed center of mass, can be calculated easily,

$$\frac{\beta F_{\mathrm{Ein}}}{N}=-\frac{3(N-1)}{2N}\ln\left(\frac{2\pi}{\beta\alpha}\right)+\frac{3\ln N}{2N}-\frac{\ln V_0}{N}+3\ln\Lambda, \tag{7}$$

where N is the total number of particles (i.e., monomers), $\beta=1/k_BT$, and $V_0=N/\rho_0$ is the volume of the system. Further, $\Lambda=h/\sqrt{2\pi mk_BT}$ is the de Broglie thermal wavelength, where m is the monomer mass and h is Plank's constant. As shown below, the final expressions for the free energy for the solid and fluid phases at equal temperatures each contain identical terms involving Λ, which, thus, plays no role in the equilibrium phase behavior; however, we retain these terms for completeness. To carry out the thermodynamic integration, we employ an effective potential,

$$\tilde{U}(\lambda)=(1-\lambda)U+\lambda U_{\mathrm{Ein}}, \tag{8}$$

where U is the internal potential energy, and where λ is a parameter employed such that $\tilde{U}(\lambda=0)=U$ and $\tilde{U}(\lambda=1)=U_{\mathrm{Ein}}$. The free energy difference between the original and reference systems may be calculated by,

$$F(\lambda=0)-F(\lambda=1)=-\int_0^1 d\lambda\left(\frac{\partial F(\lambda)}{\partial\lambda}\right)=-\int_0^1 d\lambda\left\langle\frac{\partial\tilde{U}}{\partial\lambda}\right\rangle_\lambda, \tag{9}$$

where the brackets $\langle\ldots\rangle_\lambda$ indicate an ensemble average calculated for a particular value of λ. Thus,

$$\frac{\beta F}{N}=\frac{\beta F_{\mathrm{Ein}}}{N}-\frac{\beta}{N}\int_0^1 d\lambda\langle U_{\mathrm{Ein}}-U\rangle_\lambda. \tag{10}$$

Note that in the course of the Einstein integration, the adjacent bonded beads become decoupled in the limit of $\lambda=1$. Combining Eqs. (7) and (10), we can write the total free energy per chain at $\rho_0=N/V_0$ as

$$\frac{\beta F(\rho_0)}{N_{\mathrm{ch}}}=3n\ln\Lambda-\frac{3(N-1)}{2N_{\mathrm{ch}}}\ln\left(\frac{2\pi}{\beta\alpha}\right)+\frac{3\ln N}{2N_{\mathrm{ch}}}-\frac{\ln V_0}{N_{\mathrm{ch}}}-\frac{n\beta}{N}\int_0^1 d\lambda\langle U_{\mathrm{Ein}}-U\rangle_\lambda. \tag{11}$$

The necessity of employing the fixed center-of-mass constraint is apparent from an examination of the last term in the expression above. The calculation of the free energy requires the numerical calculation of the integrand $\langle U_{\mathrm{Ein}}-U\rangle_\lambda$ for several values of λ. If the center of mass is free to diffuse with respect to the fixed Einstein crystal lattice, then this function diverges at $\lambda=0$ and, though still integrable, becomes, in practice, technically difficult to integrate.

The chemical potential at an arbitrary density can be computed using Eqs. (4), (5), and (11).

2. Fluid phase

The most convenient reference point to calculate the absolute free energy in the fluid phase is at $\rho\to0$, where the system behaves as an ideal gas of noninteracting chains. In this limit, the partition function for the system is given by,

$$Z_{\mathrm{IG}}(N_{\mathrm{ch}},V,T)=\frac{(Z_{\mathrm{ch}})^{N_{\mathrm{ch}}}}{N_{\mathrm{ch}}!}, \tag{12}$$

where Z_{ch} is the partition function for a single chain. The free energy of the ideal gas is given by,

$$\frac{\beta F_{\mathrm{IG}}}{N_{\mathrm{ch}}}=-\ln Z_{\mathrm{ch}}+\ln N_{\mathrm{ch}}!/N_{\mathrm{ch}}\approx\beta F_{\mathrm{ch}}+\ln N_{\mathrm{ch}}-1+\frac{\ln(2\pi N_{\mathrm{ch}})}{2N_{\mathrm{ch}}}, \tag{13}$$

where we have employed Stirling's formula plus the first-order correction which appears as the last term, though this turns out to be negligible even for the relatively small systems studied here. The analytical calculation of Z_{ch} and, thus, of F_{ch} for a chain with bond stretching, bond-bending and LJ interactions is a formidable problem. Instead, we define U_{id} and U_{ex},

$$U=(U_{\mathrm{stretch}}+U_{\mathrm{bend}})+U_{\mathrm{LJ}}\equiv U_{\mathrm{id}}+U_{\mathrm{ex}}, \tag{14}$$

and determine the ideal component of the single chain free energy due to the bonding interactions, $F_{\mathrm{ch}}^{\mathrm{id}}=-k_BT\ln Z_{\mathrm{ch}}^{\mathrm{id}}$, and the excess component, $F_{\mathrm{ch}}^{\mathrm{ex}}\equiv F_{\mathrm{ch}}-F_{\mathrm{ch}}^{\mathrm{id}}$, separately. The resulting expression for the ideal component of the single chain partition function, in the limit of stiff bonds, is given by

$$Z_{\mathrm{ch}}^{\mathrm{id}}=\left[\frac{4\pi V}{\Lambda^{3n}}\right]\left[\left(\frac{r_b}{\sigma}\right)^2\sigma^3\sqrt{\frac{2\pi}{\beta k_b}}\left(1+\frac{\sigma^2}{\beta k_b r_b^2}\right)\right]^{n-1}\times\left[2\pi\int_0^\pi d\theta\sin\theta\exp\left[-\frac{\beta k_\theta\theta^2}{2}\right]\right]^{n-2}, \tag{15}$$

where we have included the contribution to the partition function from the integration of the momenta. Thus, the ideal gas free energy is given by

$$\frac{\beta F_{\mathrm{IG}}}{N_{\mathrm{ch}}} = \ln(\rho/n) - 1 + \frac{\ln(2\pi N_{\mathrm{ch}})}{2N_{\mathrm{ch}}} + 3n \ln \Lambda - (n-1)\ln\left[\left(\frac{r_b}{\sigma}\right)^2 \sigma^3 \sqrt{\frac{2\pi}{\beta k_b}}\left(1 + \frac{\sigma^2}{\beta k_b r_b^2}\right)\right] - (n-2)\ln\left[2\pi \int_0^{\pi} d\theta \sin\theta \exp\left[-\frac{\beta k_\theta \theta^2}{2}\right]\right] - \ln(4\pi) + \beta F_{\mathrm{ch}}^{\mathrm{ex}}. \quad (16)$$

Using Eq. (5), and the fact that $P_{\mathrm{IG}} = N_{\mathrm{ch}} k_B T/V$, it is trivial to show that

$$\frac{\beta F(\rho)}{N_{\mathrm{ch}}} = \frac{\beta F_{\mathrm{IG}}(\rho)}{N_{\mathrm{ch}}} + \int_0^{\rho} d\rho' \left[\frac{n\beta P(\rho') - \rho'}{(\rho')^2}\right]. \quad (17)$$

The last step in the calculation of the free energy for the fluid phase is the calculation of $F_{\mathrm{ch}}^{\mathrm{ex}}$, the excess component of the single chain Helmholtz free energy arising from the intrachain LJ interactions. To this end, we adapt a Monte Carlo method developed by Frenkel *et al.*[21] based on an earlier technique due to Rosenbluth *et al.*[22] for the calculation of the excess chemical potential for continuously deformable chain molecules.

Finally, the chemical potential for the fluid phase can be calculated using Eqs. (4), (16) and (17).

C. Calculation of the phase boundaries

We use molecular dynamics (MD) computer simulations to calculate $P(\rho)$ vs ρ isotherms for the solid and fluid phases. Further, we calculate the average quantity in the Einstein integration scheme appearing in Eqs. (10) and (11) employing a ten-point Gauss-Legendre integration procedure in order to evaluate the integral. Using the expressions derived in the previous section, we can calculate the $\mu(P)$ for fixed T for each phase. The intersection of these functions determines the location where the conditions for thermodynamic coexistence are satisfied and gives a single point on the melting curve. Since the free energy calculations required to obtain this single point are computationally very expensive, we do not repeat them in order to obtain a full line of points. Instead, we employ the Gibbs-Duhem integration scheme developed by Kofke[19,20] to trace out the phase boundaries, without the need to compute further free energies. The simplest variant of this method involves the integration of the standard Claussius-Clapeyron equation,

$$\left(\frac{dP}{d\beta}\right)_{\mathrm{coexist}} = -\frac{\Delta h}{\beta \Delta v}, \quad (18)$$

where $\Delta h = h_{\mathrm{II}} - h_{\mathrm{I}}$ and $\Delta v = v_{\mathrm{II}} - v_{\mathrm{I}}$ are the differences in molar enthalpy and volume of the two phases, respectively. To implement the Kofke integration scheme, it is more convenient to rewrite Eq. (18) in the following form:

$$\left(\frac{d \ln(\beta P)}{d\beta}\right)_{\mathrm{coexist}} = -\frac{\Delta e}{\beta P \Delta v}, \quad (19)$$

where $\Delta e = e_{\mathrm{II}} - e_{\mathrm{I}}$ is the difference in molar energy between the two phases. As the Claussius-Clapeyron equation is a first-order differential equation, it can be integrated to compute the coexistence curve provided one point on the curve is known. Generally, this starting point is determined from free energy calculations, though alternative procedures, notably the Gibbs ensemble simulation method, can also provide this initial point. This latter method, however, is not applicable to the present system since it involves particle exchange between coexisting phases in separate simulation boxes. At high densities such moves become prohibitively difficult.

Finally, we note that the Kofke integration scheme is completely general and can be applied to the calculation of phase boundaries other than in ρ-T-P space. In the present study, we employ Gibbs-Duhem integration to investigate the effect of varying the chain stiffness. The Gibbs-Duhem equation for the system is

$$N_{\mathrm{ch}} d\mu = V dP - S dT + \left(\frac{\partial G}{\partial k_\theta}\right) dk_\theta. \quad (20)$$

Employing the standard criteria for thermodynamically stable coexistence between phases, and, considering the case of fixed temperature, we obtain the following relation between pressure and chain stiffness k_θ along the P-k_θ coexistence line:

$$\left(\frac{\partial P}{\partial k_\theta}\right)_{\mathrm{coexist}} = -\frac{\Delta(\partial G/\partial k_\theta)}{\Delta V}, \quad (21)$$

where $\Delta(\partial G/\partial k_\theta)$ and ΔV denote the differences in these quantities between the coexisting phases. The former quantity is given simply by,

$$\partial G/\partial k_\theta = \tfrac{1}{2} N_{\mathrm{ch}}(n-2)\langle \theta^2 \rangle, \quad (22)$$

where $\langle \theta^2 \rangle$ is the average of the square of all $N_{\mathrm{ch}} \times (n-2)$ internal bending angles in the system. Such a procedure has been used by Dijkstra *et al.*[23] to investigate the effects of chain stiffness on the nematic-isotropic phase transition of semiflexible hard spherocylinders using the rigid rod result, obtained from a Gibbs ensemble simulation, as the initial reference point.

D. Simulation details

The focus of this study is the determination of fluid-solid phase equilibrium for systems of short chain molecules. A problem associated with the simulation of the fluid phase of chain molecule systems in general is the inefficiency of the generation of significantly different system configurations required to adequately explore phase space. Recent advanced simulation techniques, such as the configurational-bias Monte Carlo (CMBC) method, provide a means to regrow, partially or completely, individual chains far more efficiently than via a completely random sampling of configurations. This method has been shown to be useful especially for long chains at moderate densities. However, since the density of the solid-fluid transition is expected to be high in the present study, this method is not expected to be particularly effective. We choose instead to employ the molecular dynamics (MD) method. We expect that following the ''natural'' dynamics of the system, in which collective motions involving

large-scale conformational changes could be important, is the most straightforward and effective approach to efficiently explore phase space. Although entanglement effects could result in sluggish dynamics for long chains, the chains studied here are sufficiently short to avoid this problem.

To calculate the isotherms for the fluid phase required for the free energy calculations described above, we perform constant-volume constant-temperature (NVT) MD simulations using a Nosé-Hoover thermostat to regulate the temperature.[24–26] We employ the reversible time-propagation integrators described by Martyna *et al.*[27] In most cases we employ a time step of $\delta t^* \equiv \delta t \sqrt{\epsilon/m\sigma^2} = 0.005$, where m is the monomer mass, and a thermostat frequency of $\omega_p^* \equiv \omega_p \sqrt{m\sigma^2/\epsilon} = 40.0$, from which the thermostat mass is given by $Q_p = N_f k_B T/\omega_p^2$, where N_f is the number of degrees of freedom.[27] We also investigated the application of multiple-time-step (MTS) methods to improve the energy conservation of the system.[27–29] In particular, we applied the reference system propagator (RESPA) technique using the bond-stretching force as the reference force. However, for the value of the associated force constant employed in most of the simulations ($k_b^* \equiv k_b \sigma^2/\epsilon = 500.0$), the time step was still short enough relative to the period of the bond-stretching vibration mode that the MTS method did not significantly improve energy conservation.

At low densities, the chains were initially aligned parallel with centers of mass on a fcc lattice stretched in the (111)-axis, and were allowed to ''melt'' into the fluid phase. However, at higher densities, the considerable hysteresis of the solid-fluid transition inhibits this process. Consequently, we compress an equilibrated low density fluid to higher density using a method due to Berendsen *et al.*[30] In this technique, the system is brought to a particular pressure by scaling the box dimensions independently at each time step in a way such that the pressure grows or decays exponentially to the desired value. The compression was performed typically in increments of $\Delta P^* \equiv \Delta P(\sigma^3/\epsilon) = 5–10$. At each pressure the fluid was typically equilibrated for a time of $\Delta t^* = 50.0–100.0$ (longer times for longer chains and higher densities), followed by production runs of comparable duration.

For systems of chains in the solid phase, we perform Parrinello-Rahman constant-stress MD simulations in which the shape, as well as the volume, of the simulation box undergoes fluctuations.[31] This method is essential for crystalline solid systems where the equilibrium crystal structure is not known *a priori*, since use of standard periodic boundary conditions, together with the imposition of a simulation box shape which is incommensurate with the unit cell of the crystal, can distort the crystal from its equilibrium structure. We employ reversible time-propagator integrators for an isothermal-isobaric ensemble derived by Martyna *et al.*[27] Further, we set the barastat frequency to $\omega_b^* = 1.0$, with the barostat mass given by $W_g = (N_f + d)k_B T/\omega_b^2 d$, where $d = 3$ is the dimensionality of the system.[27]

The equilibration of the solid phase is, in principle, much less straightforward than that of the fluid phase. In the present case, we are confronted by the problem that the LJ chains could not be crystallized from the fluid over a reasonable time scale, a process which can give some insight into the stable structure of the solid. Further, if the equilibration starts with a crystalline solid, we expect the solid to relax to a structure which is highly dependent on the initial configuration and for which there is no guarantee of thermodynamic stability. Thus, the best that can be done is to carry out equilibration runs starting from different, though sensible, initial solid structures. A free energy analysis of the resulting ''equilibrated'' metastable structures can determine which is likely to be thermodynamically stable. To choose an initial starting configuration, we make two assumptions about the structure of the stable solid. First, we assume that the chains are fully extended. We expect this to be the lowest energy single-chain configuration, with the probable exception of the fully flexible limit. Second, we assume that the chains are hexagonally packed in distinct layers. Note that both of these properties are observed in alkane solids, though the latter especially is less obviously true for the present system of semiflexible LJ chains.

We investigate the effect of initially tilting the extended chains with respect to the layer normal. In each case, the chains where aligned along the **c**-axis, one of the three vectors that define the tensor $\vec{h} = \{\mathbf{a},\mathbf{b},\mathbf{c}\}$, each of which is an edge of the parallelepiped simulation box, where the chain layers lie in the **a**-**b** plane. Initially, we set $\mathbf{a} \perp \mathbf{b}$ and $\mathbf{c}\cdot\mathbf{a} = \mathbf{c}\cdot\mathbf{b}$ and use a variety of **c**-axis tilting angles. Further, we investigated three different layer stacking configurations: (i) AAA, in which the positions of individual chains in one layer transform to those in adjacent layers by a single-layer translation along the **c**-axis; (ii) ABAB, an alternating chain-stacking structure, analogous to the hard-sphere hexagonal-close-packed (hcp) lattice stretched along the **c**-axis; and (iii) ABC, which is analogous to the hard sphere face-centered-cubic (fcc) lattice, also stretched along the **c**-axis, where the structure repeats itself every third layer. Interestingly, for the choice of parameter values used here, we find only a single ''stable'' crystal structure, regardless of the initial structure: an AAA lattice within which the **c** axis is tilted at approximately 33° with respect to the **a**-**b** plane $\cos^{-1}(\hat{a}\cdot\hat{b}) = 90°$, $\cos^{-1}(\hat{c}\cdot\hat{a}) \approx 73°$, and $\cos^{-1}(\hat{c}\cdot\hat{b}) \approx 61°$, though these values vary very slightly with temperature, chain stiffness and chain length. This structure is body-centered-cubic (BCC)-like with respect to the environment of a single monomer, with the bonded nearest neighbor sites slightly closer than the nearest nonbonded sites. While there is no other straightforward technique to prove that this structure is the thermodynamically stable one, the fact that it was the only crystal structure observed to be mechanically stable for a variety of initial starting configurations strongly suggests that it is.

In order to calculate the free energy of the solid, we compute the integral appearing in Eqs. (10) and (11) using the ten-point Gauss-Legendre quadrature method. Thus, the average energy difference $\langle U_{\mathrm{Ein}} - U \rangle_\lambda$ is evaluated for ten values of λ at constant volume. The average box shape and chain coordinates are first calculated in order to provide the reference lattice used in the Einstein integration. In the simulations used to calculate the integrand, it was found that the

use of the Nosé-Hoover thermostat was unsuitable, especially in the limit of $\lambda \to 1$, where the particles interact very weakly with each other and are strongly coupled to the lattice sites. In this limit, the system is essentially a set of decoupled harmonic oscillators, a well-known pathological case for the Nosé-Hoover method. While the problem can be avoided by using a chain of coupled Nosé-Hoover thermostats,[32] we chose instead to employ an Andersen thermostat.[33] Finally, for these simulations, we correct for the diffusion of the center of mass in the calculation of U_{Ein} in the manner described in Ref. 6.

To perform the Gibbs-Duhem integrations by integrating the pressure with respect to $\beta = 1/k_B T$ and the chain stiffness parameter k_θ via Eqs. (19) and (21), respectively, we employ the fourth-order Runge-Kutta method. Alternate integration procedures (e.g., predictor corrector) should be equally applicable. Note that the present procedure involves eight separate simulations for each time step (four for each phase) in the integrations in order to evaluate Δe and Δv in Eq. (19), and $\Delta(\partial G/\partial k_\theta)$ and ΔV in Eq. (21). While this still requires considerable computational effort to calculate a phase boundary over a reasonable range, it is still much more efficient than performing a separate free energy calculation for each point on the boundary. We employ steps of $\delta\beta^* \equiv \epsilon \cdot \delta\beta = 0.05$ and $\delta k_\theta^* \equiv (\sigma^2/\epsilon) k_\theta = 5.0$. In each case, we also performed Gibbs-Duhem integrations with larger step sizes to test the accuracy of the integration. Step sizes of double the magnitude employed here were found to give identical results.

III. RESULTS AND DISCUSSION

Snapshots of systems of semiflexible LJ chains in the fluid and solid phases are shown in Figs. 1 and 2, respectively. In each case, chains are shaded in different tones to help distinguish beads which are part of the same chain, and, in the case of Fig. 2, to distinguish chains which lie in different layers. There are six beads per chain, and 270 chains comprising the system. In Fig. 2, the origin for the tilt of the chains with respect to the layer normal in the solid phase is evident: it provides a means for the LJ beads to interdigitate with those of adjacent chains, allowing them to pack densely in layers while maintaining a low-energy extended chain conformation.

Figure 3 shows the fluid and solid branches of the $T^* \equiv k_B T/\epsilon = 2.5$ isotherm for a system of 270 six-segment chains characterized by a stiffness $k_\theta^* \equiv k_\theta \sigma^3/\epsilon = 10.0$. We note that the fluid phase of systems of LJ chains demixes into gas and liquid phases below some critical temperature, T_c^*. Using configurational-bias Gibbs ensemble-Monte Carlo (MC) simulations, Mooij *et al.*[34] have calculated the critical temperature for a system of fully flexible eight-segment LJ chains to be $T_c^* = 2.07$. Further, the value of T_c^* has been observed to decrease with decreasing number of monomers[35] and increasing stiffness.[36] Thus, the isotherm temperature is almost certainly above the critical temperature. The hysteresis in the isotherm extends over a considerable pressure range. The lowest pressure and density for the solid branch marks the approximate limit of mechanical stability of the solid phase with respect to the fluid phase. The thick horizontal line segment connecting the two branches marks the location of the equilibrium coexistence.

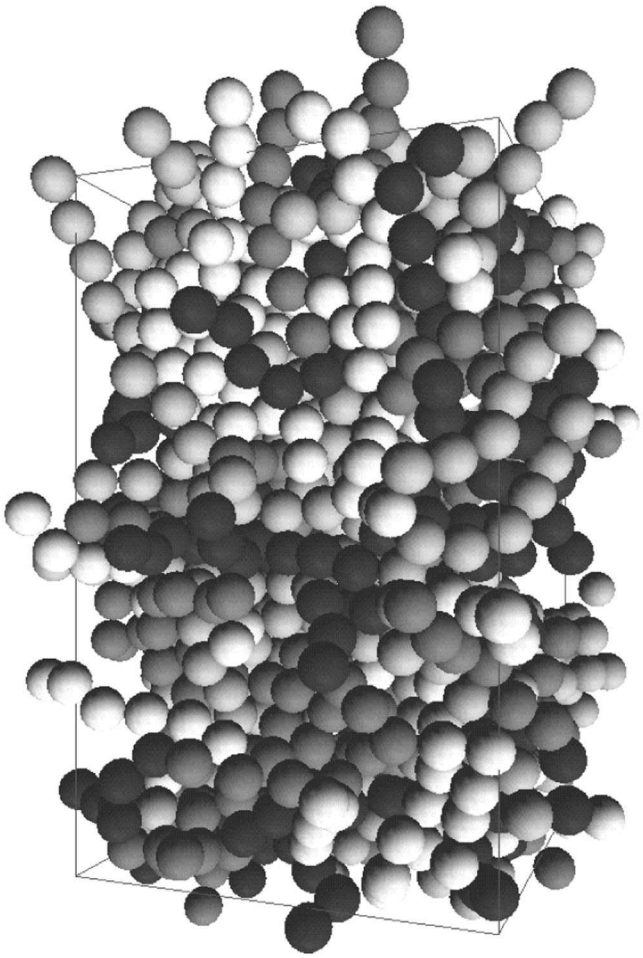

FIG. 1. Snapshot of a system of semiflexible Lennard-Jones (LJ) chains in the fluid phase near coexistence at $P^* \equiv P\sigma^3/\epsilon = 35.0$ and $T^* \equiv k_B T/\epsilon = 2.5$. The total number of chains is $N_{\mathrm{ch}} = 270$, and there are $n = 6$ LJ sites per chain. The LJ sites have been drawn as spheres with a diameter σ. Individual chains have been randomly shaded in four different tones as an aid to distinguish bonded and nonbonded sites.

To calculate the free energy of the solid phase, we employ the thermodynamic integration method outlined in Sec. II B 1. To evaluate the integral in Eqs. (10) and (11), we evaluate the integrand for ten values of λ suitable for a ten-point Gauss-Legendre integration. This is illustrated in Fig. 4, which shows a plot of $\langle \Delta u^* \rangle_\lambda \equiv \langle U_{\mathrm{Ein}} - U \rangle_\lambda / (N\epsilon)$ vs λ for the same system corresponding to Figs. 2 and 3. The solid squares define the points used in the Gauss-Legendre integration. In the measurements of $\langle \Delta u^* \rangle_\lambda$, we have set $\alpha^* \equiv \alpha\sigma^2/\epsilon = k_b^* = 500.0$. The function varies slowly for $\lambda < 0.8$, after which the slope increases to a large negative value, and the function decreases much more rapidly. This feature is due to a rapid increase in $\langle U \rangle_\lambda$ as the strength of the contribution to the potential from the internal interactions decreases, which permits more configurations with considerable overlap of the LJ beads with large positive values of $\langle U_{\mathrm{stretch}} \rangle_\lambda$ and, especially, $\langle U_{\mathrm{LJ}} \rangle_\lambda$. To ensure that this does not introduce a large contribution to the integral that is

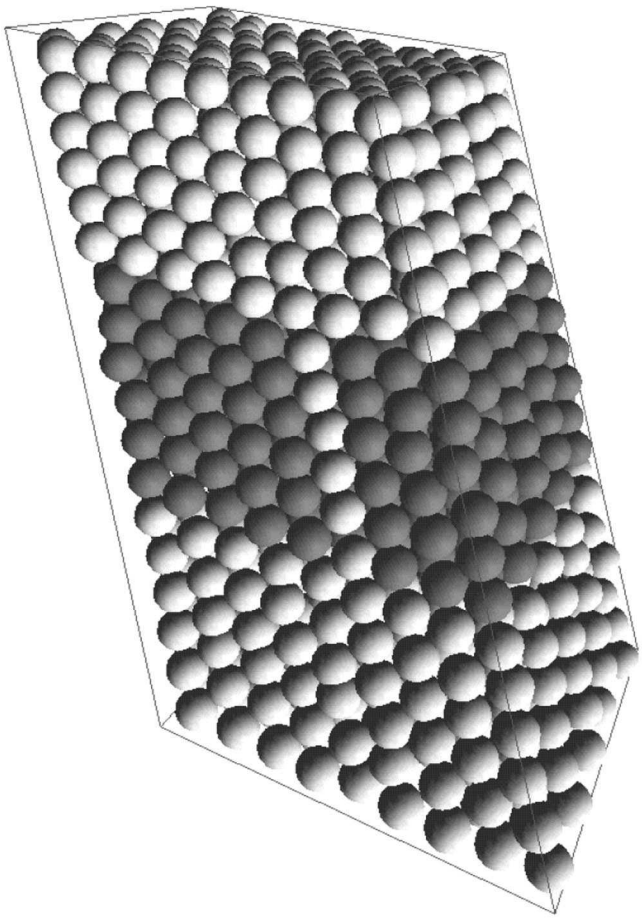

FIG. 2. Snapshot of a system of semiflexible Lennard-Jones (LJ) chains in the solid phase at $P^* \equiv P\sigma^3/\epsilon = 50.0$ and $T^* \equiv k_B T/\epsilon = 2.5$. As in Fig. 1, the total number of chains is $N_{ch} = 270$, and there are $n = 6$ LJ sites per chain. Individual chains are aligned along the longest edge of the parallelepiped simulation box. There are three layers of chains, which have been shaded in different tones as an aid to the eye. As well, one chain in the central layer has been shaded in a lighter tone to help distinguish bonded and nonbonded sites within the layer.

poorly approximated by employing an insufficient number of points, we also performed a 20-point Gauss-Legendre integration. Both calculations give identical results: $\int_0^1 d\lambda \langle \Delta u^* \rangle_\lambda = 2.81 \pm 0.01$, or $\beta(F_{Ein} - F)/N_{ch} = 6.74 \pm 0.03$.

In the system studied above, we employed a relatively weak bond-stretching constant for convenience in the simulations. However, simulations employing more realistic models for molecular systems require much stiffer bonds. We note, however, that the problem of divergences near $\lambda = 0.0$ and/or $\lambda = 1.0$ is expected to increase with increasing bond stiffness k_b. To investigate this, we have also carried out a free energy calculation on a LJ-chain solid identical to that of the previous free energy calculation, except with a bond stiffness of $k_b^* = 10\,000$, 20 times that of the previous system. Again, we fix $\alpha^* = k_b^*$. The results are shown in Fig. 5(a). In this case, there is a very strong peak at $\lambda = 0$, which could present problems for the integration. This peak is due to a rapidly increasing $\langle U_{Ein} \rangle$ due to large LJ bead displacement fluctuations transverse to the long axis of the chains when $\tilde{U} \approx U$. While decreasing the magnitude of k_b^* would reduce

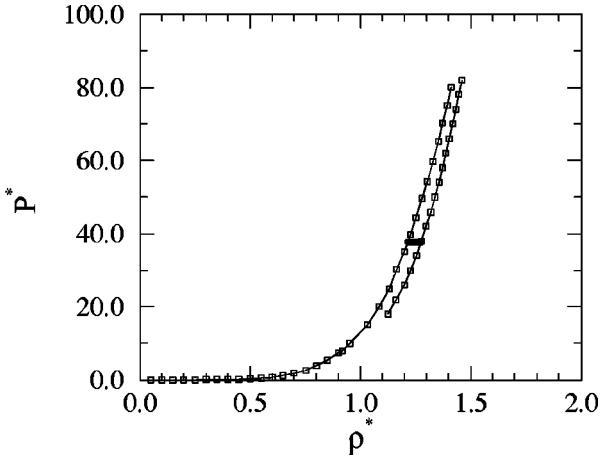

FIG. 3. Fluid and solid branches of the $T^* = 2.5$ isotherm for a system of LJ chains. The system has $N_{ch} = 270$ LJ chains of $n = 6$ LJ sites per chain. The solid horizontal line segment connecting the two branches marks the equilibrium coexistence point. The reduced pressure and density are defined as $P^* \equiv P\sigma^3/\epsilon$ and $\rho^* \equiv \rho\sigma^3$, respectively, where $\rho \equiv N/V$ is the density of monomers.

this peak, it would also induce a negative peak at $\lambda = 1$, due to large limiting values of $\langle U_{stretch} \rangle$ when bonded beads become decoupled. Another alternative would be to modify the form of U_{Ein} to employ different spring constants $\alpha_\parallel$ and $\alpha_\perp$ for directions parallel and transverse to the chain axis, and set $\alpha_\parallel^* = k_b$ and $\alpha_\perp = (\beta \langle \delta r^2 \rangle)^{-1}$. However, this approach is only relevant to this particular model of chain molecules. A more general approach is to simply change the integration variable to another such that the integrand is a more smoothly varying function. We choose the following transformation:

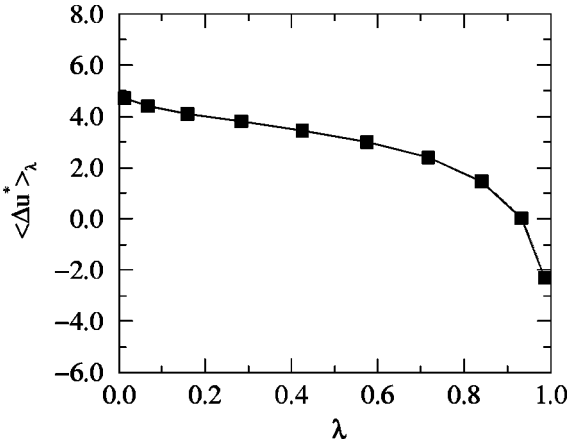

FIG. 4. Plot of $\langle \Delta u^* \rangle_\lambda$ vs λ, where $\langle \Delta u^* \rangle_\lambda \equiv \langle U_{Ein} - U \rangle_\lambda / (N\epsilon)$, and N is the number of monomers. This function appears as an integrand in Eqs. (10) and (11) and is proportional to the free energy difference between the crystalline solid phase of the LJ chain system and the reference Einstein crystal. The solid squares define the points used for a ten-point Gauss-Legendre integration. The calculation was done for a system characterized by $N_{ch} = 270$ chains, $n = 6$ segments per chain, $\alpha^* \equiv \alpha\sigma^2/\epsilon = k_b = 500.0$, $T^* \equiv k_B T/\epsilon = 2.5$, and $\rho^* \equiv \rho\sigma^3 = 1.3362$, where $\rho \equiv N/V$ is the density of monomers. The Gauss-Legendre integration yields $\int_0^1 d\lambda \langle \Delta u^* \rangle_\lambda = 2.81 \pm 0.01$, which gives $\beta(F_{Ein} - F)/N_{ch} = 6.74 \pm 0.03$.

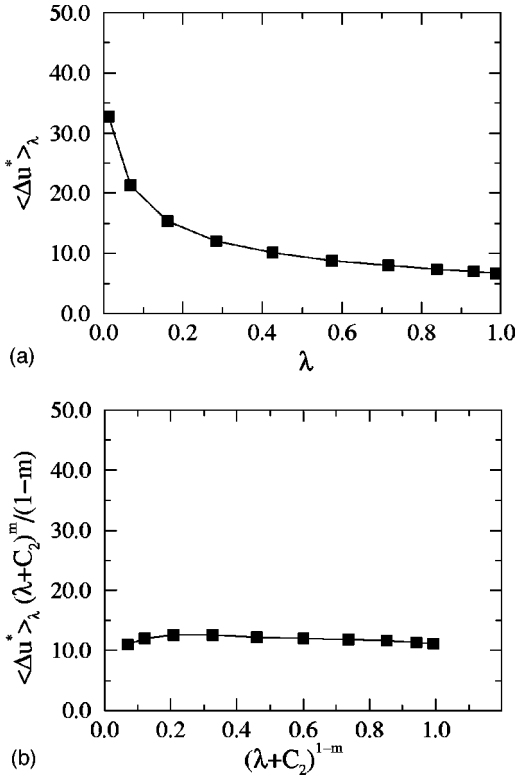

FIG. 5. (a) Plot of $\langle \Delta u^* \rangle_\lambda$ vs λ, where $\langle \Delta u^* \rangle_\lambda \equiv \langle U_{\mathrm{Ein}} - U \rangle_\lambda / (N\epsilon)$, and N is the number of monomers. The solid squares define the points used for a ten-point Gauss-Legendre integration. The calculation was done for a system characterized by $N_{\mathrm{ch}}=270$ chains, $n=6$ segments per chain, $T^* \equiv k_B T/\epsilon=2.5$, $\rho^* \equiv \rho\sigma^3=1.3151$, where $\rho \equiv N/V$ is the density of monomers, and $\alpha^* \equiv \alpha\sigma^2/\epsilon=k_b=10\,000.0$. The chain bonds are 20 times stiffer than those of Fig. 4. As a result of the high values of α^* and k_b^*, it was necessary to reduce the time step in the MD simulation from $\delta t^*=0.005$ to $\delta t^*=0.0015$. The ten-point Gauss-Legendre integration yields $\int_0^1 d\lambda \langle \Delta u^* \rangle_\lambda = 11.39 \pm 0.01$, or $\beta(F_{\mathrm{Ein}} - F)/N_{\mathrm{ch}} = 27.34 \pm 0.03$. (b) Plot of $\langle \Delta u^* \rangle_\lambda (\lambda + C_2)^m/(1-m)$ vs $(\lambda + C_2)^{1-m}$ for the same system as in (a). We choose $C_2=0.014\,66$ and $m=0.40$ to obtain a slowly varying function which is used to integrate Eq. (23). The results are identical to those of (a).

$$\int_{\lambda=0}^{1} d\lambda \langle \Delta u^* \rangle_\lambda = \int_0^1 \frac{d\lambda}{(\lambda + C_2)^m} \langle \Delta u^* \rangle_\lambda (\lambda + C_2)^m \qquad (23)$$

$$= \int_{C_2^{1-m}}^{(1+C_2)^{1-m}} d(\lambda + C_2)^{1-m} \frac{\langle \Delta u^* \rangle_\lambda (\lambda + C_2)^m}{1-m},$$

where we have chosen $C_2=0.014\,66$ and $m=0.40$. Figure 5(b) shows that the transformed integrand is a smoothly varying function of $(\lambda + C_2)^{1-m}$ and should therefore yield a better estimate of the integral than before. However, in both cases we obtain identical values of $\int_0^1 d\lambda \langle \Delta u^* \rangle_\lambda = 11.39 \pm 0.01$, or $\beta(F_{\mathrm{Ein}} - F)/N_{\mathrm{ch}} = 27.34 \pm 0.03$. This suggests that the calculation of the free energy for solids composed of chains with very stiff bonds, the case for real molecules, is relatively straightforward.

To calculate the equilibrium solid-fluid coexistence point, we require the chemical potential as a function of pressure for both phases. For the solid phase, this can be obtained from Eqs. (4), (5) and (11). The Einstein integration yields the Helmholtz free energy at one density via Eq. (11), and the measurement of the $P(\rho)$ vs ρ isotherm enables the calculation of $F(\rho)$ and $\mu(\rho)$, and, thus $\mu(P)$, from Eqs. (4) and (5). For the fluid phase, the free energy and chemical potential can be calculated with Eqs. (4), (16) and (17). The results for the $n=6$ segment system corresponding to Figs. 3 and 4 is shown in Fig. 6. Note that the chemical potential curves for each phase are very nearly parallel, i.e., the chemical potential difference between the phases varies very slowly with pressure. This is consistent with the hysteresis observed over a wide pressure range in Fig. 3, since the height of the free energy barrier between the two phases, which governs the hysteresis, is also expected to vary slowly with pressure. Finally, the intersection of the solid curve (solid phase) and the dotted curve (fluid phase), labeled by the open circle, marks the location of the coexistence point at $P^*=37.8 \pm 1$.

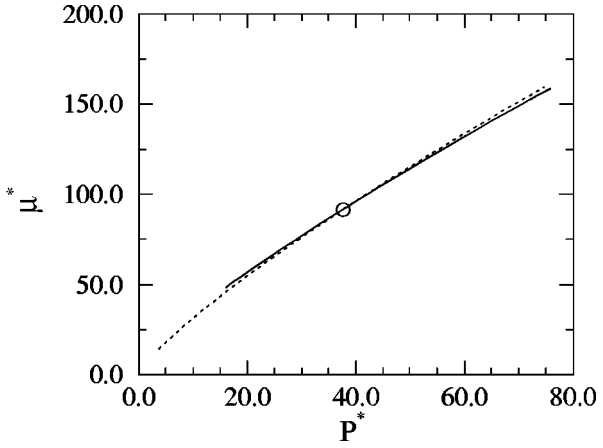

FIG. 6. Reduced chemical potential, $\mu^* \equiv \mu/\epsilon$, vs reduced pressure, $P^* \equiv P\sigma^3/\epsilon$, for the solid (solid line) and fluid (dotted line) phases of a system of LJ chains. The intersection of the two curves defines the coexistence point and is labeled by an open circle.

To calculate the complete melting curve, we integrate Eq. (19), employing the one point obtained from the free energy calculations above as the initial starting point. We have also repeated the free energy calculations above for a system of chains composed of $n=10$ monomers. Results for the two systems of $n=6$ and $n=10$ are shown in Fig. 7. Figure 7(a) shows the melting temperature as a function of pressure, and Fig. 7(b) shows the corresponding coexistence regions in the T^*-ρ^* plane. For these systems of short chains, the variation of chain length has two notable effects: (i) The melting temperature increases with increasing chain length at fixed pressure. This is consistent with experimental results for alkanes, for example, where the melting temperature is observed to increase with increasing number of methylene groups. As well, (ii) the density at the transition decreases for increasing chain length at fixed temperature.

To investigate the effect of chain stiffness on the solid-fluid phase behavior, we again employ the Gibbs-Duhem integration technique and integrate Eq. (22). The results of the calculations for systems with chain lengths of $n=6$ and $n=10$ are shown in Fig. 8. The MD simulations for the

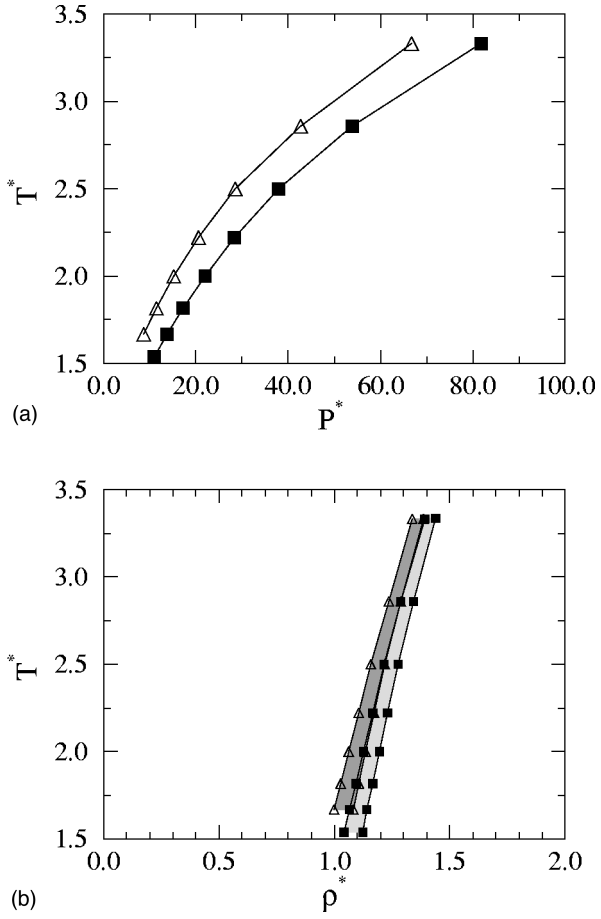

FIG. 7. (a) $T^* \equiv k_B T/\epsilon$ vs $P^* \equiv P\sigma^3/\epsilon$ melting curves for two systems of $n=6$ segment chains (solid squares) and $n=10$ segment chains (open triangles). (b) T^* vs ρ^* coexistence regions for the same systems as in (a). The curves were obtained by a numerical integration of Eq. (19) starting from an initial point at $T^*=2.5$ for each system. A fourth-order Runge-Kutta integration scheme with a step size of $\delta\beta=0.05\ \epsilon^{-1}$ was used.

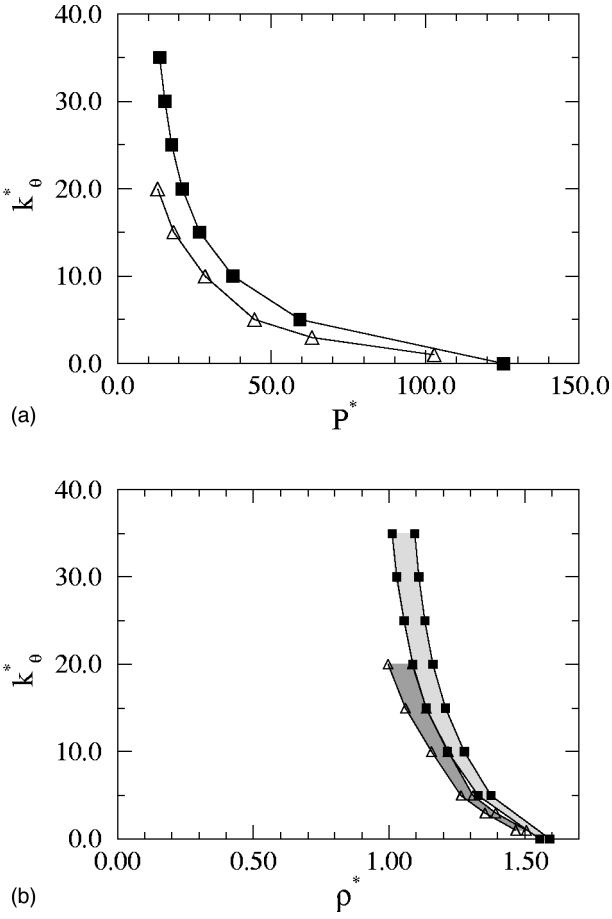

FIG. 8. (a) $k_\theta^* \equiv k_\theta \sigma^2/\epsilon$ vs $P^* \equiv P\sigma^3/\epsilon$ equilibrium melting curves for two systems of $n=6$ segment chains (solid squares) and $n=10$ segment chains (open triangles). (b) k_θ^* vs T^* coexistence regions for the same systems as in (a). The curves were obtained from a numerical integration of Eq. (21) starting from an initial point at $T^*=2.5$ obtained from a free energy calculation for each system. A fourth-order Runge-Kutta integration scheme was used, with a step size of $\delta k_\theta^*=5.0$. For the $n=10$ system, we employ step sizes of $\delta k_\theta^*=2.0$ for $k_\theta^*<5.0$.

longer chain system became very sluggish with increasing chain stiffness and could only be performed for $k_\theta^* \leqslant 20$, where $k_\theta^* \equiv k_\theta \sigma^2/\epsilon$. Figure 8(a) shows the phase boundary of the solid-fluid transition in the k_θ^*-P^* plane for $T^*=2.5$, and Fig. 8(b) shows the corresponding coexistence regions in the k_θ^*-ρ^* plane. There are three notable results: (i) Increasing the chain stiffness increases the stability of the solid phase with respect to the fluid phase in that it shifts the transition to lower pressures for fixed temperature. This effect is primarily due to an increase in the liquid phase chemical potential with k_θ^*, which, especially at lower k_θ^*, varies considerably more rapidly than the chemical potential in the solid phase. From Eqs. (20), (21) and (22), the rate of change of μ^* at constant pressure and temperature is proportional to $\langle \theta^2 \rangle$. In the solid phase, where the chains are fully extended, and, thus, where θ deviates only ever by small amounts from zero, the derivative in Eq. (22) is small. However, the chains are considerably more flexible in the fluid phase, and thus the derivative in Eq. (22) is larger. As the increase in μ^* with k_θ^* is greater for the fluid phase, the intersection of the curves shown in Fig. 6 would therefore shift to lower pressures. Table I lists the values and the ratio of values $\langle \theta^2 \rangle$ in the solid and fluid phases. Note that $\langle \theta^2 \rangle_{\text{solid}}$ is essentially independent of k_θ^*. The high ratio of $\langle \theta^2 \rangle_{\text{fluid}}/\langle \theta^2 \rangle_{\text{solid}}$ at low k_θ^* indicates a rapid increase in the coexistence pressure with k_θ^*. Note that this levels off at higher k_θ^*. (ii) Increasing the chain stiffness decreases the density at which the solid-fluid transition takes place. Note that the transition asymptotically approaches a fixed pressure and density, the rigid chain limit, as the flexibility decreases with increasing k_θ^*. (iii) The width of the coexistence region, a discontinuity which gives a measure of the strength of the first-order phase transition, also increases with increasing chain stiffness. Note that this quantity also asymptotically approaches the rigid-chain limit with increasing k_θ^*, though this is more apparent for the $n=6$ phase coexistence region which could be calculated to higher k_θ^* than that of $n=10$.

For systems like the semiflexible chains considered in this work, liquid crystal mesophases, in principle, can be thermodynamically stable for sufficiently large stiffness or low temperature. In the MD simulation studies of Wilson *et al.*[37] and Wilson,[38] a similar system of short chains, in this case composed of a string of seven hard spheres, was observed to form nematic and smectic phases for sufficiently

TABLE I. Dependence of mean-square angles $\langle\theta^2\rangle^a$ (rad^2) on chain stiffness.

n	k_θ^*	$\langle\theta^2\rangle_{\text{solid}}$	$\langle\theta^2\rangle_{\text{fluid}}$	$\langle\theta^2\rangle_{\text{fluid}}/\langle\theta^2\rangle_{\text{solid}}$
6	5	0.0396	0.7261	18.4
	10	0.0479	0.4728	9.9
	15	0.0528	0.3225	6.1
	20	0.0592	0.2344	4.0
	25	0.0569	0.1785	3.1
	30	0.0543	0.1481	2.7
	35	0.0509	0.1220	2.3
10	1	0.0635	1.087	17.1
	3	0.0550	0.914	16.6
	5	0.0623	0.695	11.2
	10	0.0661	0.450	6.8
	15	0.0697	0.329	4.7
	20	0.0692	0.251	3.6

[a]θ is the angle between adjacent bond segment vectors on the LJ chains defined in the text below Eq. (3).

stiff chains upon compression from the isotropic fluid. The isotropic-nematic transition of semiflexible hard-sphere chains was also studied recently by MC simulation[39] and theoretically,[40] where the transition was observed to shift to lower densities with increasing chain stiffness and decreasing chain length. As well, as in Refs. 37 and 38, the nematic phase was only stable for chains for sufficient stiffness. It is difficult to compare quantitatively the results of these studies with those here because of the different molecular models employed. In the present study, no orientational ordering was observed upon compression, though this could, in principle, be due to insufficiently long run times. Further, the mesophases observed for the systems of hard-sphere chains are probably less likely for the present case of semiflexible LJ chains. We expect that the presence of the attractive component of the LJ pair potential would help stabilize the solid phase with respect to any fluid mesophase; that is, the isotropic fluid is more likely to freeze to a solid upon compression or cooling rather than undergo a transition to a mesophase in the case of the LJ chains than in the case of hard-sphere chains. While we certainly do not rule out the possibility of mesophase regions in the phase diagrams of Figs. 7 and 8, we pursue the matter no further here: the principal aim of the present study is to investigate the generic effects of chain length and stiffness on the solid-fluid phase transition of a system of semiflexible chains rather than a detailed determination of the complete phase diagram for this particular model.

IV. CONCLUSIONS

In this study, we have shown that the equilibrium solid-fluid phase behavior of a system of short chain molecules can be measured using a combination of a straightforward extension of existing thermodynamic integration free energy calculation techniques and the Gibbs-Duhem integration method. In the solid phase, the free energy per chain could be measured very accurately, thus permitting an accurate determination of a point on the melting curve. We find that increasing the chain length increases the melting temperature and decreases the density at the transition. Further, we find that increasing the chain stiffness effects a stabilization of the solid phase with respect to the fluid, reducing both the pressure and density at the transition for fixed temperature, and broadens the density gap between the solid and fluid phases. Finally, we note that the methods employed here are completely general and can, in principle, be used to determine the solid-fluid phase behavior of more realistically modeled chain molecules.

Note added in proof. After the submission of this article, we became aware of a recently published paper by A. P. Malanoski and P. A. Monson [J. Chem. Phys. **107**, 6899 (1997)] on the solid-fluid phase transition for systems of fully flexible tangent hard-sphere chains, which also employs free energy calculations, and which is highly relevant to this study.

ACKNOWLEDGMENTS

This work is part of the research program of the ''Stichting Fundamenteel Onderzoek der Materie'' (FOM) and is supported by NWO (''Nederlandse Organisatie voor Wetenschappelijk Onderzoek''). We would like to thank Pieter Rein ten Wolde and Alfons van Blaaderen for a critical reading of the manuscript. J.P. acknowledges the financial support provided by the Computational Materials Science program of NWO.

[1] A. Z. Panagiotopoulos, Mol. Phys. **61**, 813 (1987).
[2] B. Widom, J. Chem. Phys. **39**, 2808 (1963).
[3] B. Widom, J. Phys. Chem. **86**, 869 (1982).
[4] W. G. Hoover and F. H. Ree, J. Chem. Phys. **47**, 4873 (1968).
[5] J. Ogura, H. Matsuda, T. Ogawa, N. Ogita, and A. Ueda, Prog. Theor. Phys. **58**, 419 (1977).
[6] D. Frenkel and A. J. C. Ladd, J. Chem. Phys. **81**, 3188 (1984).
[7] P. G. Bulhuis, D. Frenkel, S.-C. Mau, and D. A. Huse, Nature (London) **388**, 235 (1997).
[8] A. D. Bruce, N. B. Wilding, and G. J. Ackland, Phys. Rev. Lett. **79**, 3002 (1997).
[9] D. Frenkel, B. M. Mulder, and J. P. McTague, Phys. Rev. Lett. **52**, 287 (1984).
[10] D. Frenkel and B. M. Mulder, Mol. Phys. **55**, 1171 (1985).
[11] J. A. C. Veerman and D. Frenkel, Phys. Rev. A **41**, 3237 (1990).
[12] P. G. Bulhuis and D. Frenkel, J. Chem. Phys. **106**, 666 (1997).
[13] E. J. Meijer, D. Frenkel, R. A. LeSar, and A. J. C. Ladd, J. Chem. Phys. **92**, 7570 (1990).
[14] B. Kuchta, K. Rohleder, R. D. Etters, and J. Belak, J. Chem. Phys. **102**, 3349 (1995).
[15] B. Kuchta, K. Rohleder, D. Swanson, and R. D. Etters, J. Chem. Phys. **106**, 6771 (1997).
[16] B. Kuchta and R. D. Etters, Phys. Rev. B **47**, 14 691 (1993).
[17] B. Kuchta and R. D. Etters, Phys. Rev. B **45**, 5072 (1992).
[18] L. A. Báez and P. Clancy, Mol. Phys. **86**, 385 (1995).
[19] D. A. Kofke, Mol. Phys. **78**, 1331 (1993).
[20] D. A. Kofke, J. Chem. Phys. **98**, 4149 (1993).
[21] D. Frenkel, G. C. A. M. Mooij, and B. Smit, J. Phys.: Condens. Matter **3**, 3053 (1991).
[22] M. N. Rosenbluth and A. W. Rosenbluth, J. Chem. Phys. **23**, 356 (1955).
[23] M. Dijkstra and D. Frenkel, Phys. Rev. E **51**, 5891 (1995).
[24] S. Nosé, Mol. Phys. **52**, 255 (1984).
[25] S. Nosé, J. Phys. Chem. **81**, 511 (1984).
[26] W. G. Hoover, Phys. Rev. A **31**, 1695 (1985).
[27] G. J. Martyna, M. E. Tuckerman, D. J. Tobias, and M. L. Klein, Mol. Phys. **87**, 1117 (1996).

[28] M. Tuckerman, G. J. Martyna, and B. J. Berne, J. Chem. Phys. **93**, 1287 (1990).
[29] M. Tuckerman, B. J. Berne, and G. J. Martyna, J. Chem. Phys. **97**, 1990 (1992).
[30] H. J. C. Berendsen, J. P. M. Postma, W. F. van Gunsteren, A. DiNola, and J. R. Haak, J. Chem. Phys. **81**, 3684 (1984).
[31] M. Parrinello and A. Rahman, Phys. Rev. Lett. **45**, 1196 (1980).
[32] G. J. Martyna, M. L. Klein, and M. E. Tuckerman, J. Chem. Phys. **97**, 2635 (1992).
[33] H. C. Andersen, J. Chem. Phys. **72**, 2384 (1980).
[34] G. C. A. M. Mooij, D. Frenkel, and B. Smit, J. Phys.: Condens. Matter **4**, L255 (1992).
[35] Y.-J. Sheng, A. Z. Panagiotopoulos, S. K. Kumar, and I. Szleifer, Macromolecules **27**, 400 (1994).
[36] Y.-J. Sheng, A. Z. Panagiotopoulos, and S. K. Kumar, Macromolecules **29**, 4444 (1996).
[37] M. R. Wilson and M. P. Allen, Mol. Phys. **80**, 277 (1993).
[38] M. R. Wilson, Mol. Phys. **81**, 675 (1994).
[39] F. A. Escobedo and J. J. de Pablo, J. Chem. Phys. **106**, 9858 (1997).
[40] H. Fynewever and A. Yethiraj, J. Chem. Phys. **108**, 1636 (1998).